**RESEARCH PAPER**

# Combined effects of wall slip and nanofluid on interfacial transport from a thin-film evaporating meniscus in a microfluidic channel

Ritesh Dwivedi[1] · Sukumar Pati[2] · Pawan K. Singh[1]

## Abstract
An improved comprehensive semi-analytical model is devised and postulated to unveil the underlying physics of thin-film evaporating dynamics in a microfluidic channel using $Al_2O_3$ water nanofluid as working liquid with/without porous coating layer of nanoparticles. The model uses the mass transport equation based on the kinetic theory and the Young–Laplace equation for pressure differential and incorporates the slip boundary condition on the wall of the channel. It reveals that the wall slip is a crucial parameter that increases the cumulative heat transfer with decreased thickness of the thin-film evaporating meniscus. Furthermore, mainly three volume fractions 0.5%, 1%, and 2% has been considered in the present work and it is observed that nanofluid plays an important role in the increment of heat flux which is about 31% with the volume fraction of 2% and 25 nm diameter particles when only enhanced thermophysical properties are considered without slip. However, it exaggerates the results by 29% when porous coating layer of nanoparticles is neglected. It is also noticed that a porous coating layer deposited by the nanoparticles can even reduce the heat transfer phenomenon. Moreover, for a given combination of nanoparticle diameter and volume fraction, increase in the thermal resistance may reach up to an extent that even increased thermal conductivity cannot counteract it and hence, the heat transfer obtained using nanofluid can be worse than the heat transfer obtained using the base liquid water alone.

**Keywords** Thin-film evaporation · Heat transfer · Wall slip · Nanofluid · Disjoining pressure · Porous coating layer

## List of symbols

| | |
|---|---|
| $A$ | Dispersion constant, J |
| $C_a$ | Accommodation coefficient |
| $D$ | Constant |
| $d$ | Diameter, m |
| $h_l$ | Latent heat of vaporization, J/kg |
| $K_p$ | Permeability of the porous coating layer, $m^2$ |
| $k$ | Conductivity (thermal), W/m K |
| $k_B$ | Boltzmann's constant, $1.38 \times 10^{-23}$ J/K |
| $\dot{m}_x$ | Mass flow rate of liquid/width, kg/m s |
| $m_{ev}$ | Evaporative mass flux, $kg/m^2$ s |
| $\tilde{M}$ | Molecular weight, kg/mol |
| $P$ | Pressure, Pa |
| Pr | Prandtl number |
| $q''$ | Heat flux, $W/m^2$ |
| $R_c$ | Interfacial radius of curvature, m |
| $\tilde{R}$ | Universal gas constant, J/mol K |
| Re | Reynolds number |
| $t_{nl}$ | Thickness of nanolayer, m |
| $T$ | Temperature, K |
| $\Delta T$ | Wall superheat, K |
| $u$ | Velocity along $x$-direction, m/s |
| $V_l$ | Molar volume of bulk liquid, $m^3/mol$ |
| $x, y$ | $x$- and $y$-coordinate, respectively, m |

### Greek symbols

| | |
|---|---|
| $\alpha$ | Ratio in Eq. 32 |
| $\beta$ | Slip coefficient |
| $\gamma$ | Constant |
| $\chi$ | Ratio in Eq. 32 |
| $\delta$ | Thin-film thickness, m |
| $\delta_0$ | Film thickness of non-evaporating region, m |
| $\delta'$ | First derivative |
| $\delta''$ | Second derivative, $m^{-1}$ |
| $\mu$ | Dynamic viscosity, Pa s |
| $\varepsilon$ | Porosity |
| $\nu$ | Kinematic viscosity, $m^2/s$ |

✉ Pawan K. Singh
pawan@iitism.ac.in

1 Department of Mechanical Engineering, Indian Institute of Technology (ISM) Dhanbad, Dhanbad, Jharkhand 826004, India

2 Department of Mechanical Engineering, National Institute of Technology Silchar, Silchar 788010, Assam, India

$\rho$     Density, kg/m$^3$

$\sigma$     Surface tension coefficient, N/m

$\phi$     Volume fraction of nanoparticles

**Subscripts**

cp     Capillary

dp     Disjoining

e     Equivalent

l     Liquid

net     Net effective

nl     Nanolayer between nanoparticle and base liquid

p     Nanoparticles

pw     Porous coating layer at wall

$\delta i$     Vapor–liquid interface

v     Vapor

w     Wall

# 1 Introduction

Miniaturization of electronic devices and their perceptible use in wide range of applications arouse the undeniable curiosity of scientific community to explore and delineate the essential physics involved with the micro- and nanoscale two-phase thermal transport processes to curb the heat transfer problems. In this context, thin-film evaporation, a phase change technique like in loop heat pipe or capillary pumped loop, can be looked upon as an encouraging solution because of its capability to transfer heat in a manifold when compared to the single-phase heat transfer phenomena (Wayner 1973; Holm and Goplen 1979). The exposure of a wetting liquid on to the surface of a microchannel (like water on fused silica) formed an extended meniscus, as illustrated in Fig. 1. The extended meniscus can be categorized into three regions, each exhibiting distinct characteristics. The first one is the adsorbed region, where no evaporation occurs due to large intermolecular force between liquid and surface. The second one is the thin-film evaporation region, where
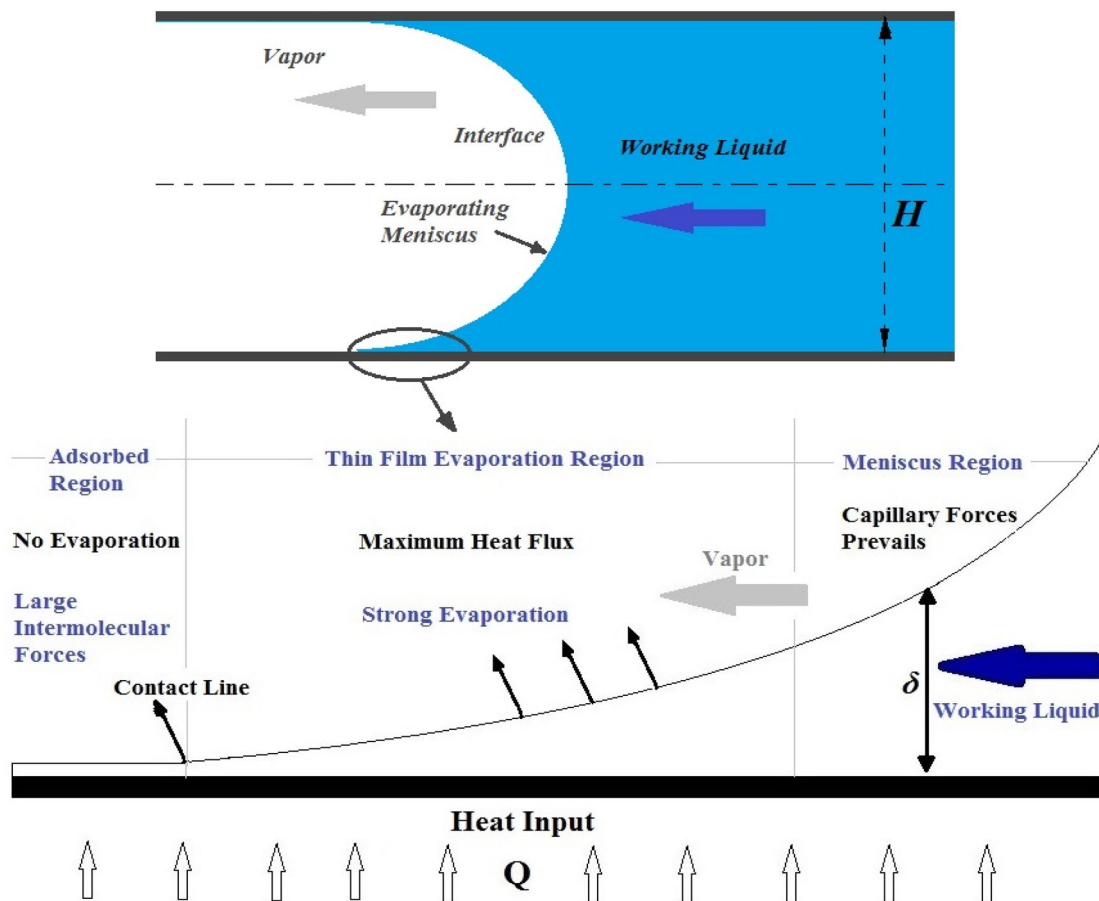


**Fig. 1** Schematic of thin-film evaporation in a microfluidic channel, $H$ is the height of the channel, $\delta$ is thickness of the evaporating thin film, and $Q$ is the heat input

maximum evaporation occurs with a combined effect of disjoining pressure ($P_d$) and capillary pressure ($P_c$) and the final one is the meniscus region, where limited rate of evaporation occurs due to dominance of capillary pressure. It is important to note that several researchers opted for different conditions to specify the thin-film region. In this framework, Park et al. (2003) considered that the thin-film region lies within the range from maximum $P_d$ to $P_d \geq P_c$, while Wang et al. (2007) suggested that the thin-film region ranges from maximum $P_d$ to $P_{dp} = 1/5000$ of $P_{dp}|_{x = 0}$. In addition to this, it is also revealed in their study that for constant wall superheat, if the size of the microchannel varies, the thickness at the end of the thin film remains invariant, and the length of the thin-film region may vary, but, inconsequentially. However, for constant channel size, the topology of the thin film varies strongly with the wall superheat.

Potash and Wayner (1972) first formulated the mathematical model to depict the evaporation process from a thin-film evaporating meniscus in a two-dimensional microfluidic channel and revealed that the prerequisite pressure gradient for the fluid flow from the thin-film region is due to the change in the profile of meniscus, i.e., capillarity effect and the gradient of the disjoining pressure. Later, Truong and Wayner (1987) experimentally investigated the equilibrium profile of the meniscus and examined the effect of van der Waals forces and capillary forces on the same. They also concluded that length of the evaporating thin film varies in micrometers. To quantify the mass transport at the vapor–liquid interface, Schrage (1953) developed a mathematical model which was later used by many articles to predict the thermal characteristics of an evaporating thin film in a microfluidic channel. For example, Wang et al. (2007) thoroughly investigated the implications of the evaporating meniscus and expound the rudimentary facets of thin-film region after considering the Schrage model with uniform vapor pressure. On contrary to this, Park et al. (2003) considered the vapor pressure gradient along with the interfacial shear stress to encapsulate the fluid flow behavior and the heat transfer process in thin-film evaporation.

Kou and Bai (2011) explicated the evolution of the solid–liquid interface to predict the effect of temperature jump and wall slip. They concluded that both mass and heat transport can be reduced by decreasing the degree of superheat due to the wall slip and temperature jump. Similarly, Lim and Hung (2015) suggested that nullifying the thermocapillary effect, due to temperature gradient, may overestimate the heat and mass transport. Later, different analytical and numerical techniques have been analysed and compared by Kou et al. (2015). They concluded from their numerical investigation that if interfacial temperature is obtained from the Clausius–Clapeyron equation in comparison with Wayner's model to predict the mass flux, it will lead to overrated heat transfer. Since then, a plethora

of work both numerical and experimental (DasGupta et al. 1993; Chakraborty and Som 2005; Jiao et al. 2005; Suman 2008; Ma et al. 2008; Sait and Ma 2009; Narayanan et al. 2009; Biswal et al. 2011; Kundu et al. 2011; Hanchak et al. 2016a, b) has been made in this area to get acquainted with the underlying physics of the evaporating meniscus. Even a little while back, evaporation of thin liquid film over a nanostructured surface and at the base of a fin have also been estimated theoretically (Hu and Sun 2016; Mandel et al. 2017). The profile of the extended meniscus and the heat transport process in the thin-film region affects significantly due to the differential pressure of the bulk vapor flow (Fu et al. 2018). In addition to this, in spite of the fact that classic conjecture of no-slip is appropriate and sufficient to predict the macroscale transport problems, it leads to the unrealistic results when it comes to the microscopic levels (Gad-el-Hak 2001; Tretheway and Meinhart 2002). Although several investigations have been conducted in the regime of thin-film evaporation, only few of them (Park et al. 2003; Wee et al. 2005; Gatapova and Kabov 2007; Panchamgam et al. 2008; Pati et al. 2013) have considered the effect of wall slip till now. It is important to note that in the context of thin-film evaporation, the steady-state of the evaporation can be maintained by the large pressure gradient only. Furthermore, the slip boundary condition, which depends upon this large pressure gradient increases the slip velocity; therefore, the slip cannot be ignored for the accurate modeling of the physics. Moreover, the experimental and theoretical exploration of Panchamgam et al. (2008) suggested that an agreement between the heat dissipation from the substrate and the evaporation of the fluid from the meniscus can be obtained only if a due consideration is given to a slip velocity at the solid–liquid interface. Wee et al. (2005) suggested that slip boundary conditions at wall can enhance the heat and mass flux, while decreases the viscous drag. They also concluded that slip effect is more pronounced when superheat is increased. Biswal et al. (2011) investigated the consequences of the interfacial slip and concluded that depleted gas layer above the wall surface can increase the net evaporative mass flux as well as the thickness of the evaporating liquid film. Furthermore, Pati et al. (2013) also revealed that the evaporation of the thin liquid from the nanopores always exaggerates the results if not given the due consideration to the interfacial slip. Therefore, the present study assesses the effect of wall slip to delineate the realistic physics of the evaporating thin-film region.

Working liquid, being an important parameter in heat transfer, can also alter the physics of an evaporating meniscus and thus, nanofluid becomes the center of attraction and entices the research community because of its salient features (Choi and Eastman 1995; Xuan and Li 2000; Hwang et al. 2009). Nanofluid is an amalgamation of nano-size particles (metallic or non-metallic) suspended

in the base liquid (Lee et al. 1999). It has been noticed that nanofluid can increase the thermophysical properties of the working liquid particularly thermal conductivity (Ozerinc et al. 2010; Fan and Wang 2011; Tesfai et al. 2012; Dwivedi and Singh 2018; Tiwary et al. 2019). Do and Jang (2010) suggested in their study that the inclusion of nanofluid as a working medium can enhance the thermal performance of the heat pipes. Later, Poplaski et al. (2017) revealed in their theoretical study that although the overall thermal resistance of the heat pipe reduces due to the enhanced thermal conductivity, the effect of nanoparticle deposition and incorporation of nanolayer formation is must for accurate modeling. In context of thin-film evaporating meniscus, Zhao et al. (2011) discussed the effect of nanofluid on thin-film evaporation after considering the theoretical model opted by Park et al. (2003) and the enhanced thermophysical properties due to the nanoparticles. However, they neglected the wall slip effect and considered only the effect of interfacial shear stress at the vapor–liquid and the gradient in the vapor pressure. Interestingly, Hanchack et al. (2014, 2016a, b), on the contrary, conducted the experimental and theoretical investigations on the evaporating thin liquid film based on the Schrage model (1953) with uniform vapor pressure and no shear stress at the vapor–liquid interface. The results obtained from their theoretical formulation compliments the experimental findings and hence suggested that using kinetic-theory based mass transport model is more plausible and practical in solving problems. Recently, Dwivedi and Singh (2019) showed the effect of nanofluid in context of thin-film evaporation using a semi-analytical model based on the kinetic-theory based mass transport equation. It has been revealed in their study that the use of nanofluid increases the heat transfer rate from evaporating thin-film regions. However, study of the effect of the slip at the wall surface and the porous coating layer of the nanoparticles was beyond the scope of their study. Moreover, considering only the enhanced thermophysical properties due to nanofluid inclusion may over/under-estimate the heat transfer and thus require to incorporate the effect of porous coating layer of nanoparticles to get the clear facet of the effect of nanofluid on the evaporating meniscus. Nanoparticles' self-structuring and their stratification over the solid wall can create a hindrance in the heat transfer process (Nikolov et al. 2010). Several researchers have showed that during the evaporation process, the surface morphology of the heat transfer surface has been altered in case of nanofluid (Liu et al. 2007a, b). It has also been revealed that these nanoparticles covered the surface and formed a thin porous coating layer over the evaporation region (Chon et al. 2007). Hence, it becomes radical to incorporate the consequences and implications of the porous coating layer over the wall surface. However, to the best of author's knowledge, no study has been made in this context till now delineating the mechanistic understanding of a evaporating thin-film region after encapsulating the consequences of wall slip as well as the effect of the nanofluid as working liquid with/without porous coating layer of nanoparticles.

Accordingly, objective of the current study is to develop an improved comprehensive semi-analytical model using the kinetic-theory for the mass transport equation and Young–Laplace equation for the pressure differential to elucidate the critical and essential insight of the evaporating meniscus in context of evaporation and heat transfer for nanofluid (water–$Al_2O_3$) from a microfluidic channel. This study is used to first investigate the effect of wall slip and later the combined effect of enhanced thermophysical properties and a porous coating layer of nanoparticles on a thin-film evaporating meniscus in a microfluidic channel. The variation in different parameters such as thin-film thickness ($\delta$), heat flux ($q''$), evaporative mass flux ($m_{ev}$), disjoining pressure ($P_{dp}$), and cumulative heat transfer per unit width ($Q_{cum}$) has been used to illuminate the physics of the thin-film evaporating meniscus for different nanoparticle diameters and volumetric concentrations.

## 2 Mathematical modeling

This section describes the mathematical model used to predict the transport phenomenon at the vapor–liquid interphase of an extended meniscus from a two-dimensional microfluidic channel. Only the zoomed view of the lower half section has been considered here due to the symmetry of the channel, as illustrated in Fig. 2. The heat is supplied from both sides of the channel and nanofluid completely wets the wall of the channel which is maintained at a uniform temperature $T_w$. The meniscus is superheated with dry saturated vapor maintained at a temperature $T_v$ and a uniform pressure $P_v$. The present analysis has been done on the following assumption –

(a) The flow in the microfluidic channel is two-dimensional, laminar, and steady-state (Biswal et al. 2011).
(b) Temperature and liquid pressure gradient is present only along y-coordinate and x-coordinate, respectively (Wang et al. 2007; Dwivedi and Singh 2019).
(c) No shear stress exists at vapor–liquid interface (Hanchak et al. 2014).
(d) Heat transfer in the liquid is solely due to conduction with negligible convective term in momentum equation (Moosman and Homsy 1980; Ranjan et al. 2011).
(e) Nanofluid is a single-phase mixture with constant latent heat and surface tension as of base fluid (Do and Jang 2010; Zhao et al. 2011).
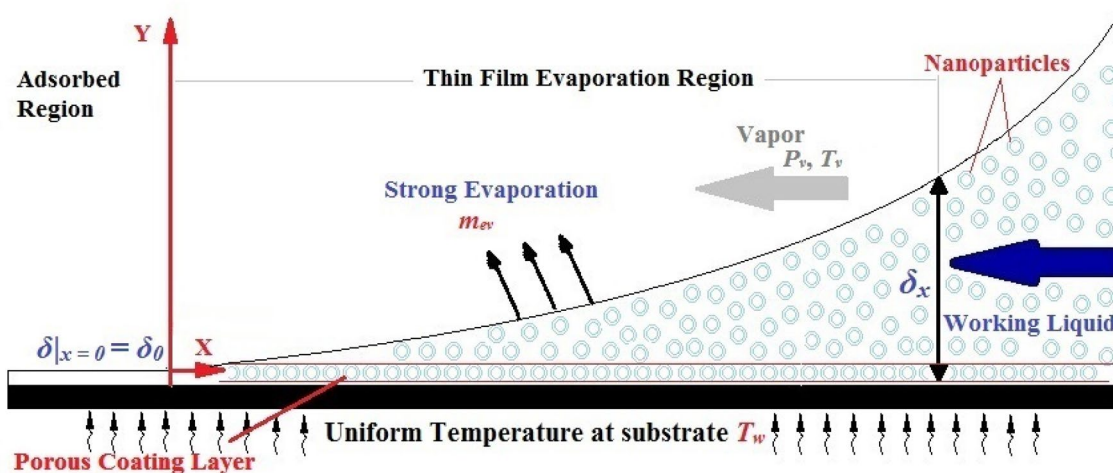
**Fig. 2** Coordinate system and schematic of thin-film evaporation region with porous coating layer of nanoparticles, $m_{ev}$ is the evaporative mass flux

The necessary pressure gradient required to advance the fluid flow can be obtained by the Young–Laplace equation as a summation of capillary and disjoining pressure (Wayner et al. 1976), given by

$$P_v - P_l = P_{cp} + P_{dp}, \tag{1}$$

where $P_v$ and $P_l$ are the vapor and liquid pressure, respectively. The capillary and disjoining pressure can be further given as

$$P_{cp} = \frac{\sigma}{R_c}, \quad R_c = \frac{\left(1 + \delta'^2\right)^{1.5}}{\delta''} \quad \text{and} \quad P_{dp} = \frac{A}{\delta^3}. \tag{2}$$

In the above equation, $\sigma$ and $R_c$ are the surface tension coefficient and interfacial radius of curvature, respectively, $\delta'$ and $\delta''$ represent the first and second order derivatives of the thickness, and $A$ is the dispersion constant. The Young–Laplace equation is further used to obtained the evaporative mass flux $m_{ev}$, based on the kinetic-theory, proposed by Wayner (1973), Wayner et al. (1976), Truong and Wayner (1987) and Schonberg et al. (1995), as follows:

$$m_{ev} = C_a \left(\frac{\tilde{M}}{2\pi \tilde{R} T_{\delta i}}\right)^{1/2} \frac{P_v}{\tilde{R} T_{\delta i}} \left[\frac{\tilde{M} h_l}{T_v}\left(T_{\delta i} - T_v\right) - V_l\left(P_v - P_l\right)\right], \tag{3}$$

where $C_a = 2.0$ is the accommodation coefficient. The molecular weight and the universal gas constant of the working liquid are represented by $\tilde{M}$ and $\tilde{R}$, respectively, $V_l$ is the molar volume, and $h_l$ is the latent heat of vaporization of the base liquid. In above equation, the interfacial temperature $T_{\delta i}$ of the vapor–liquid interface with varying thickness is represented and given by using the Clausius–Clapeyron

equation (Ma et al. 2008; Zhao et al. 2011; Yan and Ma 2013; Dwivedi and Singh 2019) as

$$T_{\delta i} = T_v \left(1 + \frac{P_v - P_l}{\rho_v h_l}\right). \tag{4}$$

The total mass transfer through evaporation can also be obtained by employing the conservation of mass for the differential length $dx$ in the axial direction of the evaporating thin film, to yield

$$m_{ev} = -\frac{d\dot{m}_x}{dx}, \tag{5}$$

where

$$\dot{m}_x = \int_0^\delta \rho_{net} u_l \, dy. \tag{6}$$

Here, $\dot{m}_x$ is the rate of mass flow along the axial direction for unit width, and $\rho_{net}$ is the net effective density of the working liquid. Furthermore, for very low Reynolds number in narrow confined geometries, conservation of momentum can be used to obtain the velocity profile $u_l$ through lubricant theory, given as

$$\frac{\partial^2 u_l}{\partial x^2} = \frac{1}{\mu_{net}} \frac{dP_l}{dx}, \tag{7}$$

where $\mu_{net}$ is the net effective viscosity of the working liquid and double integration of Eq. (7) with the given boundary conditions can represent the velocity profile.

Case A: For effective wall slip

At, $y = 0$, $u_1 = \beta \dfrac{du_1}{dx}$, (8a)

$y = \delta$, $\dfrac{\partial u_1}{\partial y} = 0$, (8b)

where $\beta$ is the slip coefficient, and $\delta$ is the thin-film thickness of the evaporating meniscus. Hence, the velocity profile is obtained as

$$u_1 = \frac{1}{\mu_{net}} \frac{dP_1}{dx}\left(\frac{y^2}{2} - y\delta - \beta\delta\right).$$ (9)

Therefore, on combining Eqs. (5), (6) and (9), $m_{ev}$ can be obtained as

$$m_{ev} = \frac{d}{dx}\left(\frac{\delta^3 + 3\beta\delta^2}{3\nu_{net}}\frac{dP_1}{dx}\right),$$ (10)

where $\nu_{net}$ is the net effective kinematic viscosity of the working liquid.

Case B: For nanofluid

At, $y = 0$, $u_1 = u_{pw} = \dfrac{1}{\mu_{net}}\dfrac{dP_1}{dx}K_p$, (11a)

$y = \delta$, $\dfrac{\partial u_1}{\partial y} = 0$, (11b)

where $u_{pw}$ is the average velocity of nanofluid with a porous coating layer at the wall, and $K_p$ is the permeability of the porous coating layer. The expressions for the $u_{pw}$ and $K_p$ can be obtained from the one-dimensional Darcy equation to incorporate the effect of porous coating layer of nanoparticles (Do and Jang 2010; Zhao et al. 2011), as

$$\frac{dP_1}{dx} = \frac{\mu_{net}u_{pw}}{K_p} \text{ and } K_p = \frac{\varepsilon^3}{180(1-\varepsilon)^2}d_p^2,$$ (12)

where $\varepsilon$ is the porosity of the randomly packed uniform sized sphereical nanoparticles and $d_p$ is the size or the average diameter of the nanoparticles. Using Eqs. (11a–12) the velocity profile yields to

$$u_1 = \frac{1}{\mu_{net}}\frac{dP_1}{dx}\left(\frac{y^2}{2} - y\delta + K_p\right).$$ (13)

Hence, evaporative mass flux in case of nanofluid incorporation can be obtained using Eqs. (5–6) and (13), it follows

$$m_{ev} = \frac{d}{dx}\left(\frac{\delta^3 - 3K_p\delta}{3\nu_{net}}\frac{dP_1}{dx}\right).$$ (14)

Now, for Case B, as assumed that the heat is transported in the liquid solely due to conduction, it can be given in the form of heat flux by employing the conservation of heat transfer, as

$$q'' = m_{ev}h_1 = \frac{T_w - T_{\delta i}}{\underbrace{\dfrac{\delta}{k_{net}} + \dfrac{\delta_c}{k_c}}_{R_{th}}},$$ (15)

where $k_{net}$ is the net effective thermal conductivity of the working nanofluid and $\delta_c$ and $k_c$ are the thickness and the thermal conductivity of the coated layer of the nanoparticles, respectively. In addition, $R_{th}$ represents the total thermal resistance through conduction, where second term of the $R_{th}$ is due to the porous coating layer of the nanoparticles, where $k_c$ is given by (Do and Jang 2010; Zhao et al. 2011)

$$k_c = \left[4\ln\left(\frac{k_p}{k_1}\right) - 11\right]k_1,$$ (16)

where $k_p$ and $k_1$ are the thermal conductivity of individual nanoparticle and base liquid, respectively. Furthermore, $m_{ev}$ and $T_{\delta i}$ the interfacial temperature can be obtained from Eqs. (14) and (4), respectively, and by substituting it in Eq. (15), one may write

$$h_1\frac{d}{dx}\left(\frac{\delta^3 - 3K_p\delta}{3\nu_{net}}\frac{dP_1}{dx}\right) = \frac{T_w - T_v\left(1 + \frac{P_v - P_1}{\rho_v h_1}\right)}{\frac{\delta}{k_{net}} + \frac{\delta_c}{k_c}}.$$ (17)

In the above equation, the gradient of liquid pressure can be obtained from Eqs. (1–2). However, it has been noticed that it is disjoining pressure which dominates and plays a nontrivial contribution in the thin-film region over the capillary force which prevails after the beginning of the intrinsic meniscus region (Wayner et al. 1976; Schonberg and Wayner 1992; Yan and Ma 2013; Dwivedi and Singh 2019). Therefore, in the immediate work, since disjoining pressure plays a vital role we neglect the term capillary pressure and assume that the gradient of the liquid pressure arises due to the gradient of the disjoining pressure alone. Hence, by combining and solving Eqs. (1–2) for identical vapor pressure and incorporating it in Eq. (17), we obtain

$$\frac{A}{\nu_{net}}\frac{d}{dx}\left(\frac{\delta^3 - 3K_p\delta}{3\nu_{net}}\delta'\right) = \frac{1}{h_1}\frac{T_w - T_v\left(1 + \frac{A}{\rho_v h_1 \delta^3}\right)}{\frac{\delta}{k_{net}} + \frac{\delta_c}{k_c}}.$$ (18)

Rearranging the above equation yields to

$$\frac{d}{dx}\left(\frac{\delta^2 - 3K_p}{\delta^3}\delta'\right) = \frac{B}{R_{th}} - \frac{C}{R_{th}\delta^3},$$ (19)

where, $B = \dfrac{\mu_{net}(T_w - T_v)}{\rho_{net} A h_l}$, $C = \dfrac{\mu_{net} T_v}{\rho_{net} \rho_v h_l^2}$. $\qquad$ (20)

Moreover, in non-evaporating adsorbed region, the large intermolecular forces curb the thickness of the thin liquid film to a minimum and hence the interfacial temperature $T_{\delta i}$ of the contact line becomes equivalent to the temperature of the wall $T_w$. Therefore, the initial thickness of the extended meniscus is obtained using Eqs. (1–2) and (4) and on comparing it with Eq. (19) it is observed:

$$\frac{C}{B} = \frac{A T_v}{\rho_v h_l (T_w - T_v)} = \delta_0^3. \qquad (21)$$

On solving Eqs. (15) and (19–20) analytically, heat flux can be determined as

$$q'' = \frac{A h_l}{v_{net}} \frac{d}{dx}\left(\frac{\delta^2 - 3K_p}{\delta^3}\delta'\right) = \frac{A h_l}{v_{net}} \frac{B}{R_{th}}\left(1 - \frac{C}{B\delta^3}\right). \qquad (22)$$

Furthermore, heat flux is obtained by combining Eqs. (20–21) and substituting into Eq. (22). Hence, given as

$$q'' = \frac{T_w - T_v}{\frac{\delta}{k_{net}} + \frac{\delta_c}{k_c}}\left(1 - \frac{\delta_0^3}{\delta^3}\right). \qquad (23)$$

The calculation of the heat flux in Eq. (23) has been done for Case B with inclusion of porous coating layer. However, the same analytical procedure can be opted out to obtain the heat flux for Case A. The only difference while solving the heat flux for Case A is that the evaporating mass flux will be different and obtained from Eq. (10) and there will be no extra thermal resistance term in $R_{th}$. Therefore, the heat flux for Case A is found as

$$q'' = \frac{T_w - T_v}{\frac{\delta}{k_{net}}}\left(1 - \frac{\delta_0^3}{\delta^3}\right). \qquad (24)$$

The thickness of the evaporating thin film can be determined using the mass transport based kinetic theory as given in Eq. (3) and the total mass transfer through the evaporation obtained by differentiating Eqs. (10) and (14) for the case of effective wall slip and incorporation of nanofluid, respectively. Accordingly

$$\text{Case A: } m_{ev} = \frac{A}{v_{net}}\left(\frac{\delta\delta'' - \delta'^2}{\delta^2} + \frac{3\beta\delta^2\delta'' - 6\beta\delta\delta'^2}{\delta^4}\right), \qquad (25)$$

$$\text{Case B: } m_{ev} = \frac{A}{v_{net}}\left(\frac{\delta\delta'' - \delta'^2}{\delta^2} - \frac{3K_p\delta\delta'' - 9K_p\delta'^2}{\delta^4}\right). \qquad (26)$$

Equations (25) and (26) are acquired after considering the effect of wall slip and a porous coating layer of nanoparticles at the wall. However, to apply the classical notion of no-slip boundary condition, we can take the value of $\beta$ or $K_p$ as zero in either equation. Now, the thin-film thickness can be found using these Eqs. (25–26) along with Eq. (3) for different conditions such as for no-slip; wall slip effect; nanofluid with effect of only enhanced thermophysical properties; nanofluid with enhanced thermophysical properties and porous coating layer of nanoparticles.

As seen in the above expressions, a non-linear ordinary differential equation of second order has been obtained and hence the Runge–Kutta method is employed to solve the aforementioned equations. The initial conditions have been opted at the intersection of the adsorbed and thin-film evaporation region at $x = 0$. Since there is no evaporation prior to the intersection, the interfacial temperature and the wall temperature will be identical ($T_{\delta i} = T_w$) and the evaporative mass flux $m_{ev}$ will be zero. In addition, the initial thickness of thin-film profile can be obtained from Eq. (21) as $\delta_0 = 1.75 \times 10^{-8}$ m, where all the properties of water were calculated at $T_v = 333$ K. However, this calculation has been obtained by considering no evaporation, which implies at the adsorbed region. Therefore, a slightly higher value of $\delta_0 = 2 \times 10^{-8}$ m is considered here at the intersection of the adsorbed region and thin-film region. The first derivative of thin-film thickness represents the slope and cannot be zero, thus taken as $\delta' = 10^{-11}$ m. The expanse of the thin-film evaporation region has been decided by the significance of the disjoining pressure. As disjoining pressure almost nullifies in the beginning of the meniscus region; therefore, the thin-film evaporation region is considered up to $P_{dp} = 1/3000$ of $P_{dp}|_{x=0}$.

The nontrivial interplay of nanoparticles directly affects the thermophysical properties of the working liquid and subsequently the evaporating process in the thin-film region. Furthermore, it has been noticed that enhanced dynamic viscosity and density can be postulated on the basis of the experimental explorations; however, formalism of enhanced thermal conductivity may vary according to the nature of the system especially in microfluidic channels (Shima et al. 2009). Therefore, the net effective density and the dynamic viscosity of the nanofluid (or working liquid) can be estimated directly as (Ozerinc et al. 2010; Singh et al. 2010)

$$\rho_{net} = \phi\rho_p + (1 - \phi)\rho_l, \qquad (27)$$

$$\mu_{net} = \mu_l(1 + 10\phi), \qquad (28)$$

where $\phi$ and $\mu_l$ are the volumetric concentration of the nanoparticles and the dynamic viscosity of the base liquid, $\rho_p = 3880$ kg/m$^3$ and $\rho_l$ are the density of the nanoparticles and base liquid, respectively.

The model used to predict the enhanced thermal conductivity in the immediate work is based on two conjectures, i.e., effect of liquid layering around the nanoparticles and effect of the Brownian motion. Moreover, for spherical nanoparticles, there exists a thin nanolayer between the nanoparticle and the base liquid and contributed collectively in the enhancement of the thermal conductivity, given as (Yu and Choi 2003)

$$k_{net} = \frac{2k_l + 2(k_e - k_l)\phi_e + k_e}{2k_l - (k_e - k_l)\phi_e + k_e}k_l, \tag{29}$$

where $\phi_e$ and $k_e$ are the equivalent volumetric fraction and thermal conductivity of the nanoparticles, respectively, and given as

$$\phi_e = \phi(1 + \chi)^3, \tag{30}$$

and

$$k_e = \frac{\alpha[(1 + 2\alpha)(1 + \chi)^3 + 2(1 - \alpha)]}{(1 + 2\alpha)(1 + \chi)^3 - (1 - \alpha)}k_p, \tag{31}$$

where $\alpha = \frac{k_{nl}}{k_p}$ and $\chi = \frac{2t_{nl}}{d_p}$. $\tag{32}$

Here, $d_p$ is the diameter of the nanoparticle, and $k_{nl}$ and $t_{nl}$ represents the thermal conductivity and thickness of the nanolayer between the nanoparticles and base fluid, respectively. In above expression, $k_p$ is given by (Chen 1996)

$$k_p = \frac{3d_p}{3d_p + 8t_{nl}}k_b, \tag{33}$$

where $k_b = 42.34$ W/m K, is the bulk thermal conductivity of $Al_2O_3$ naoparticles. The enhanced thermal conductivity predicted by Eq. (29) is in situ until used for the room temperature conditions, since increment in the temperature may differ the value of thermal conductivity anomalously (Das et al. 2003). It has been noticed that increased temperature directly increases the Brownian motion and hence the energy transport and microconvection effect. Therefore, to correctly predict the enhanced thermal conductivity, effect of Brownian motion due to increased temperature has been incorporated and estimated as (Jang and Choi 2004; Shima et al. 2009)

$$k_{brwn} = D\frac{d_l}{d_p}k_l Re^{\gamma} \; Pr^{0.333} \; \phi_e, \tag{34}$$

where $Re = \frac{1}{v_l}\sqrt{\frac{18k_B T}{\pi \rho_p d_p}}, \tag{35}$

where $D$ and $\gamma$ are the constants ($D = 2.55 \times 10^6$, $\gamma = 2.5$), $d_l$ and Pr is the molecule diameter and the Prandtl number of the base liquid, respectively, and Re is the Reynolds number of the nanoparticle. In addition, $k_B$ represents the Boltzmann's constant.

Therefore, on combining Eqs. (29) and (34), the net enhanced thermal conductivity of the nanofluid can be found as

$$k_{net} = \frac{2k_l + 2(k_e - k_l)\phi_e + k_e}{2k_l - (k_e - k_l)\phi_e + k_e}k_l + k_{brwn}. \tag{36}$$

Now, Eqs. (27), (28), and (36) are available with the enhanced thermophysical properties of the working liquid, especially nanofluid, to predict the thickness of the evaporating meniscus from Eqs. (25) or (26) and consequently, the heat flux from Eqs. (23) or (24).
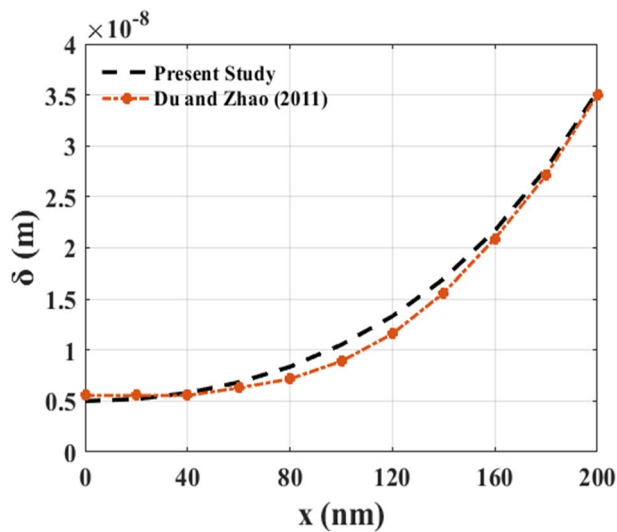
## 3 Results and discussion

The objective of this study is to explore the characteristics of the evaporating thin-film region in a microfluidic channel using nanofluid as working liquid with/without porous coating layer of nanoparticles. An amalgamation of water and alumina is considered as nanofluid. This section includes the comparison of its effect on the evaporating thin-film region with the base liquid incorporating the slip effect at the wall, in terms of $\delta$, $P_{dp}$, $T_{\delta i}$, $q''$, $m_{ev}$, and $Q_{cum}$. The wall is heated uniformly at $T_w = 335$ K with 2 K of wall superheat ($\Delta T$) and average diameter of the nanoparticle is considered 25 nm with three different volumetric concentrations, $\phi = 0.5\%$, 1%, and 2% to accumulate the effect of nanofluid (water + $Al_2O_3$). Thermophysical properties of the water can be obtained from Table 1.

The validation of the improved semi-analytical model is illustrated in Fig. 3. However, the literature survey unveiled that no study has been reported till now delineating the attributes pertaining to the evaporating meniscus, especially thin-film evaporation region after encapsulating the consequences of wall slip as well as the effect of the nanofluid as working liquid with/without porous coating layer of

**Table 1** Properties of water and operating parameters

| Properties of liquid | Values |
|---|---|
| $A$ (J) | $1 \times 10^{-20}$ |
| $h_l$ (J/kg) | $2.358 \times 10^6$ |
| $k_l$ (W/m K) | 0.653 |
| $\rho_l$ (kg/m³) | 983.28 |
| $\mu_l$ (N-s/m²) | $4.63 \times 10^{-4}$ |
| $T_v$ (K) | 333 |
| $\rho_v$ (kg/m³) | 0.13020 |

**Fig. 3** Comparison of the results obtained by present analytical model and the model presented by Du and Zhao for superheat 1 K and $T_v = 333$ K

nanoparticles. To the best of author's knowledge, this is the first work analyzing the combined effect of wall slip as well as the effect of the nanofluid as working liquid with/without porous coating layer of nanoparticles on the transport characteristics of a thin-film region. Accordingly, there is no scope for validation of the results of the current work with the results reported in literature. However, the correctness of the adopted methodology is ascertained by comparing the results of the thickness of the thin-film evaporation region with the results reported in the literature Du and Zhao (2011) for superheat 1 K and $T_v = 333$ K. It can be inferred from Fig. 3 that both the models for the variation in the thickness of the thin-film evaporation region are following the same

trend, and the dispersion constant might be the possible reason for the slight differences.

### 3.1 Thin-film characteristics for base liquid

Figure 4 depicts the variation of thickness and disjoining pressure in thin-film region along the axial direction for the base liquid, i.e., water, without considering slip at the wall. As seen in figure, the liquid film is almost flat near the adsorbed region due to strong intermolecular attraction between wall and liquid and later, the thickness of the thin film increases and makes a steeper slope as approaching towards the meniscus region. Disjoining pressure, as shown in Fig. 4b, is also maximum at the inception of the thin-film region due to the large intermolecular force and feeble down continuously in the axial direction as the thin-film thickness increases. Beyond this point, the capillary forces prevail and the region between the maximum and minimum magnitude of the disjoining pressure is termed as thin-film evaporation region. Therefore, the expense of the thin-film evaporation region can be resolved through the variation in the disjoining pressure. Here, length of the thin-film region is obtained as 350 nm. Furthermore, all other parameters in this study were examined for the same length.

The pictorial representation in Fig. 5 illustrates the variation of interfacial temperature and evaporating mass flux with respect to the film thickness. It is inferred from Fig. 5a that the temperature near the adsorbed region is maximum and then drops suddenly with the increment in the thickness and becomes constant along the meniscus. In addition, more than 90% of the temperature drop occurs within 50 nm thickness. Moreover, it can be noticed from Fig. 5b that there is no mass transfer until $0.2 \times 10^{-7}$ m thickness. This can be perceived in a way that at first, near the adsorbed
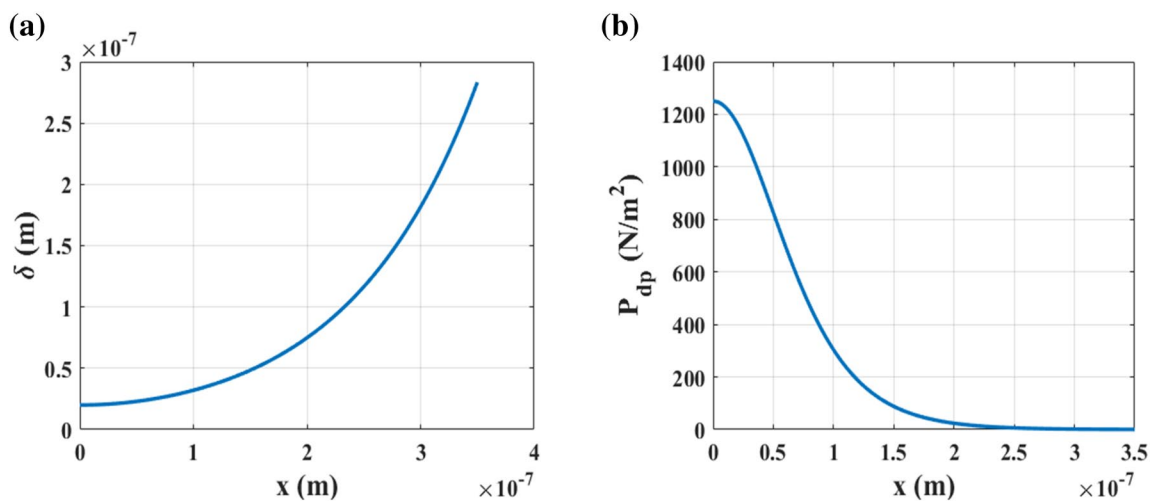


**Fig. 4** Variation of **a** thickness and **b** disjoining pressure in thin-film region along the axial direction for base liquid water without slip

**(a)**

**(b)**
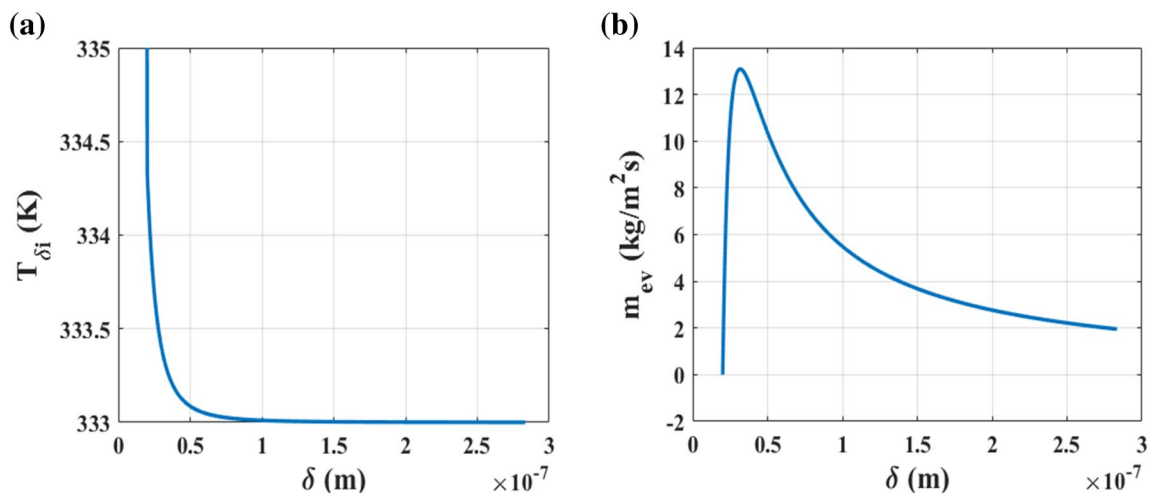
Fig. 5 Variation of **a** interfacial temperature and **b** evaporative mass flux with respect to the thickness for water without slip

region, dominance of the disjoining pressure is so large that evaporation near this region is oppressed by the intermolecular forces. Furthermore, this force between the solid–liquid interfaces declines with the advancement in the axial direction and thus gives sudden rise to the mass transfer such that evaporation starts taking place and increases with an increase in the thin-film thickness. It is heeded that the evaporative mass flux reaches its apex limit within a very short range of thickness from 20 to 50 nm and declines with further increment in the thickness due to the increment in the capillary pressure as well as the high thickness of the thin film.

Heat flux, as obtained from Eq. (24) is illustrated in Fig. 6a. It is observed that heat flux is zero near the adsorbed region and reaches the maximum value with the increment

in the axial direction because of the increase in the degree of the wall superheat ($T_w - T_{\delta i}$). However, after reaching the apex value, although the temperature difference is still higher but there is a slump decrement in the heat flux with further increment in the thickness in the axial direction. This can be inferred in a way that increase in the thickness of thin film directly increases the thermal resistance $R_{th}$ of the thin film; therefore, there exists a point, where heat flux is maximum and then decreases with further increment in the thickness due to an increase in the thermal resistance. The axial variation of cumulative heat transfer per unit width ($Q_{cum} = \int_0^x q'' \mathrm{d}x$) is depicted in Fig. 6b. It is conceived that maximum amount of heat transfer occurs within the evaporating thin-film region only and after entering meniscus region, the contribution to the total heat transfer reduces

**(a)**

**(b)**
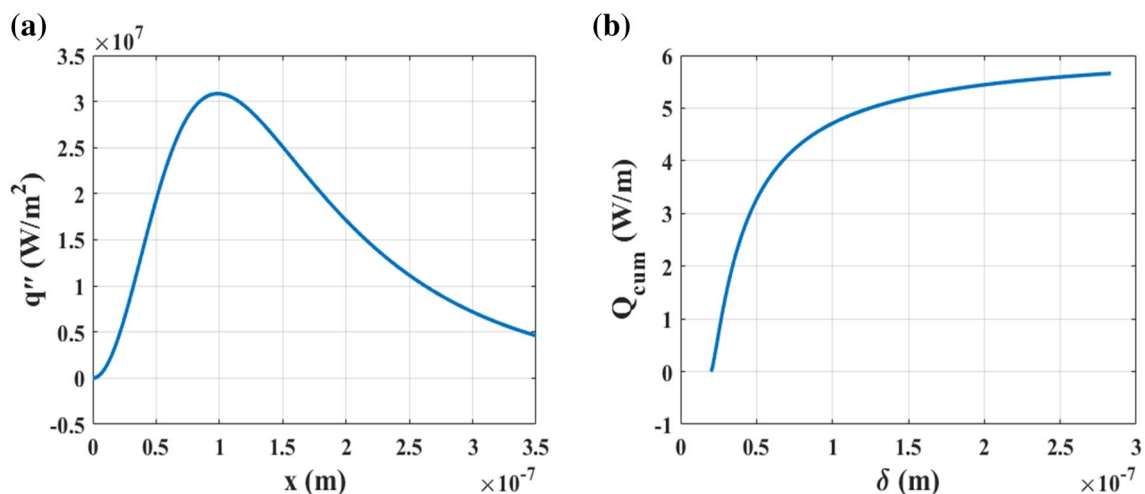
Fig. 6 Variation of **a** heat flux along the axial direction and **b** cumulative heat transfer with the thin-film thickness for water without slip

and hence only slight change in the slope can be noticed thereafter. Moreover, it can be inferred from the figure that more than 60% of the overall heat transfer takes place within the evaporating thin-film region which is in line with the findings of Wang et al. (2007).

## 3.2 Effect of wall slip

The effect of the slip at wall is depicted in Fig. 7. In the context of thin-film evaporation, several researchers (Park et al. 2003; Wee et al. 2005; Shkarah et al. 2015; Pati et al. 2013) have considered concave meniscus with fluid–solid interfacial slip having slip coefficient in the range of 1–10 nm and accordingly, the value of slip coefficient ranging from 1 to 5 nm is used in the current work. The shape of the evaporating meniscus is illustrated in Fig. 7a and shows the comparison between no-slip and slip boundary conditions. It can be clearly seen from the figure that for slip

condition, the length of the thin-film region increases and thickness of the thin liquid decreases implying that the net effective area available for the interfacial transport in thin-film region increases. Thus, a slight shifting of the heat flux and disjoining pressure curve can be noticed in Fig. 7b, c, respectively. In addition, the decreased thickness of thin liquid film suggests the increase in disjoining pressure in case of slip flow as compared to no-slip condition. Interestingly, although, the heat flux does not show any notable change in the magnitude; however, the cumulative heat transfer increases significantly with respect to thickness, for the increased length of the thin-film region, as observed in the pictorial representation of Fig. 7d. It is noticed that the cumulative heat transfer increases by about 1.5%, 4%, and 7% when slip at wall is considered with $\beta = 1$ nm, $\beta = 3$ nm, and $\beta = 5$ nm, respectively, in comparison with the no-slip classical conjecture. This can be attributed to the fact that slip at the wall can mitigate the viscous drag and intrinsically
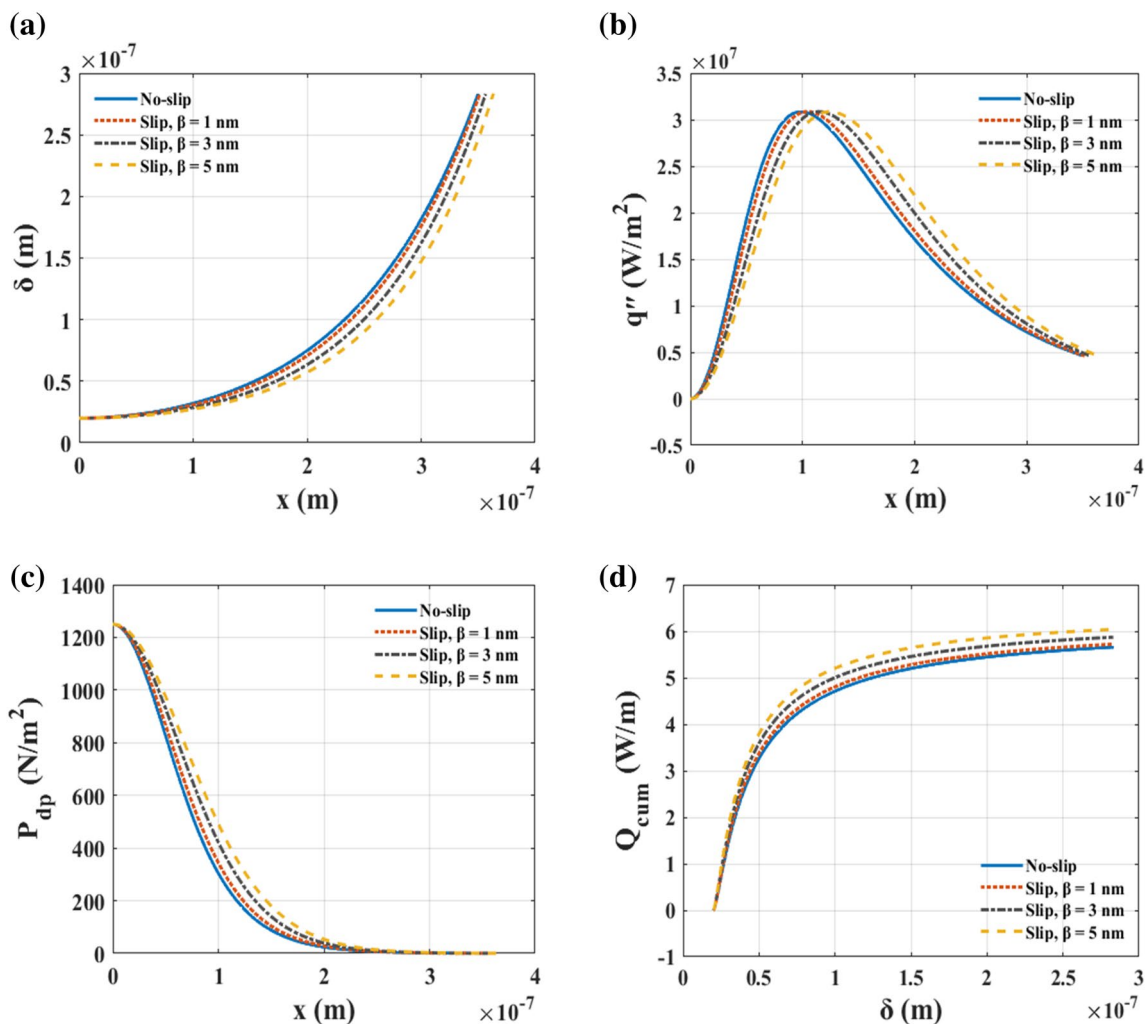


**Fig. 7** Effect of wall slip on **a** thickness, **b** heat flux, **c** disjoining pressure, **d** cumulative heat transfer in thin-film evaporating meniscus, with $\beta = 0$, 1, 3, and 5 nm

the resistance to the flow, which leads to an increased velocity at the liquid–solid interface. Therefore, the length of the thin-film region increases with increased disjoining pressure and reduced thickness at a given position when compared to no-slip condition. Furthermore, the lesser resistance offers at the solid–liquid interface now renders more flow of bulk liquid into the evaporating thin-film region. Consequently, the effective wall slip enhances the spreading of the working liquid, and increases the cumulative heat transfer. Accordingly, it is important to give the due consideration to the effect of wall slip while accumulating the adequate characteristics of the thin-film region.

### 3.3 Effect of nanofluid

Figure 8 depicts the effect of the enhanced thermophysical properties of nanofluid on thin evaporating meniscus without consideration of slip and the results are compared with the base liquid. The illustrated figure also neglects the effect of the porous coating layer of nanoparticles. It is noticed that thickness (refer Fig. 8a) and the heat flux (refer Fig. 8b) can be increased using nanofluid in comparison with the water as base fluid. The value of increased thermal conductivity, maximum thickness of the thin film, and maximum heat flux are mentioned in Table 2. Inclusion of nanofluid shows that for average nanoparticle diameter $d_p = 25$ nm, thickness of the thin film increases by 5.54%, 11.08%, and 22.27% as $\phi$ increases by 0.5%, 1%, and 2%, respectively. Similarly, heat flux also increases by 7.64%, 15.29%, and 30.66% with the increase in $\phi$ of 0.5%, 1%, and 2%, respectively. Therefore, it can be said that for the same length of the thin-film region, incorporation of nanofluid makes significant increment in the magnitude of the heat flux with a small change in the shape of the evaporating meniscus. Moreover, the evaporative mass flux and the cumulative heat transfer shows the increment of 7%, 15%, and 30% and 6%, 12%, and 23%,
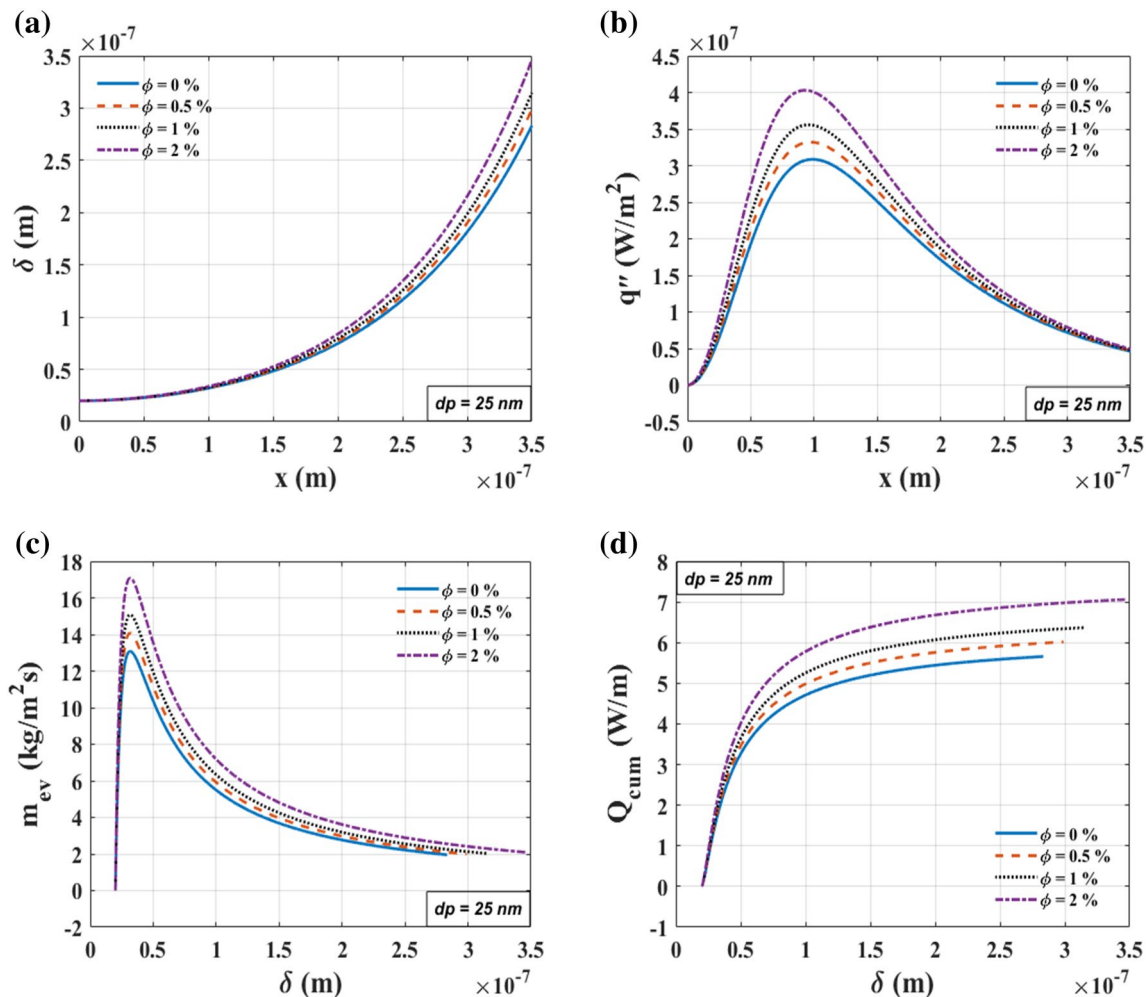


**Fig. 8** Effect of enhanced thermophysical properties of nanofluid with different volumetric fractions ($\phi$) at a given average diameter of nanoparticles ($d_p$) and without porous coating layer on **a** thickness, **b** heat Flux, **c** evaporative mass flux, **d** cumulative heat transfer of thin-film region

**Table 2** Effect of enhanced thermophysical properties of nanofluid ($d_p = 25$ nm)

| Volume fraction ($\rightarrow$) | 0% | 0.5% | 1% | 2% |
|---|---|---|---|---|
| $k_{net}$ (W/mK) | 0.653 | 0.702 | 0.752 | 0.853 |
| $\delta_{max}$ (m) | $2.833 \times 10^{-7}$ | $2.990 \times 10^{-7}$ | $3.147 \times 10^{-7}$ | $3.464 \times 10^{-7}$ |
| $q''_{max}$ (W/m$^2$) | $3.085 \times 10^{7}$ | $3.321 \times 10^{7}$ | $3.557 \times 10^{7}$ | $4.031 \times 10^{7}$ |

respectively, using nanofluid for the volume fraction 0.5%, 1%, and 2% in comparison with water alone, as depicted in Fig. 8c, d.

It is observed from Eq. (23) that heat flux also depends on the thermal conductivity of the working liquid and increment in the thermal conductivity is observed as 7.50%, 15.16%, and 30.62% for the volume fraction of 0.5%, 1%, and 2%, respectively. In addition, the ratio of the thermal conductivity of the nanofluid water–Al$_2$O$_3$ and the base liquid *water* is obtained as 1.07, 1.15, and 1.30, respectively. In this regard, an important observation that can be made is that the increase in the thin-film thickness is very small as compared to increase in the heat flux implying that although, thickness of thin film increases with nanofluid inclusion; however, overall thermal resistance tends to decrease because of the fact that increased thermal conductivity surpasses the percentage increase in the thin-film thickness. It is also quite interesting to note that the percentage increment in the net effective thermal conductivity and the percentage increment in the heat flux is directly proportional suggesting that $k_{net}$ is more pronounced and enhances the heat transfer from the evaporating thin-film region rather than net effective density and viscosity of the nanofluid. Accordingly, it can be inferred from the above discussion that enhanced thermophysical property due to the inclusion of nanoparticle in the base fluid, particularly thermal conductivity, can enhance the heat transfer significantly without making a significant alteration in the shape of the evaporating meniscus when slip condition and layer of porous coating of nanoparticles has been neglected.

Figure 9 shows the effect of the porous coating layer of nanoparticles and the enhanced thermophysical properties together with the effect of the size of the nanoparticle diameter on the heat flux. It can be clearly seen in Fig. 9a that heat flux, in case of nanofluid with the consideration of porous coating layer of nanoparticles along with the enhanced thermophysical properties, is even less as compared to the case of pure water. Heat flux decreases by 11.73% when nanoparticle of $d_p = 25$ nm is used with 0.5% volumetric concentration as a nanofluid in comparison with water. This happens because of the increase in net thermal resistance due to the porous coating layer (in Eq. 23). It is important to mention here that the thickness of porous coating $\delta_c$ is considered identical to the size of the nanoparticles $d_p = 25$ nm and the comparisons of nanofluid are made with water without slip boundary condition. It can be mentioned in this context that

the deposition of nanoparticles is a transient phenomenon that depends also upon the solubility of the nanoparticles and prior estimation of the thickness of the porous coating layer is a difficult task as far as the theoretical modeling is considered. However, the minimum possible thickness is the single layer of the nanoparticles which is identical to the size of the nanoparticles. Accordingly, in the present study the thickness of porous coating layer ($\delta_c$) is considered same as the size of the nanoparticles. It is apparent from Fig. 9b that heat flux can be increased using the nanofluid with $d_p = 25$ nm by overcoming the net thermal resistance for higher volumetric fraction $\phi = 3\%$. It is found that net heat flux is increased by 12.73% when nanofluid is used in comparison with water. For the given condition, the nanofluid incorporation exaggerates the increase in heat flux by 29.58% when only enhanced thermophysical properties are considered with no porous coating layer of nanoparticles.

The amount of heat transfer from the evaporating meniscus also depends on the size of the nanoparticles as can be inferred from Fig. 9c, d. It is observed that when size of the nanoparticles reduces from 25 to 13 nm, the net heat flux with porous coating layer can be increased even at a lower volume fraction of $\phi = 0.5\%$. For small size of nanoparticle $d_p = 13$ nm, the effective heat flux with porous coating layer is increased by 10.76%; however, enhanced thermophysical properties alone suggested that heat flux is increased by 34% which is an overestimate of the actual value, as shown in Fig. 9c. In this context, it is observed that for the same volumetric fraction $\phi = 0.5\%$, inclusion of nanofluid may reduce the heat transfer (for $d_p = 25$ nm) or increase the heat transfer (for $d_p = 13$ nm) when porous coating layer is included. This is because, as diameter or size of the nanoparticle decreases, heat transfer increases and vice versa. Figure 9d illustrates that for constant volume fraction $\phi = 1\%$, as we reduce the nanoparticle's size from 30 nm to 20 nm and then 15 nm, the heat transfer increases. This can be elucidated in a way that as the size of the nanoparticle reduces, it allows more number of nanoparticles to accumulate for the same volume fraction and hence, transfers more heat through microconvection energy transport.

Figure 10 shows the effective cumulative heat transfer from the evaporating meniscus in thin-film evaporation region and compare the results after considering the effect of wall slip ($\beta = 5$ nm) as well as the nanofluids incorporation with the porous coating layer. The illustrated figure shows that for large size of nanoparticles ($d_p = 25$ nm), one
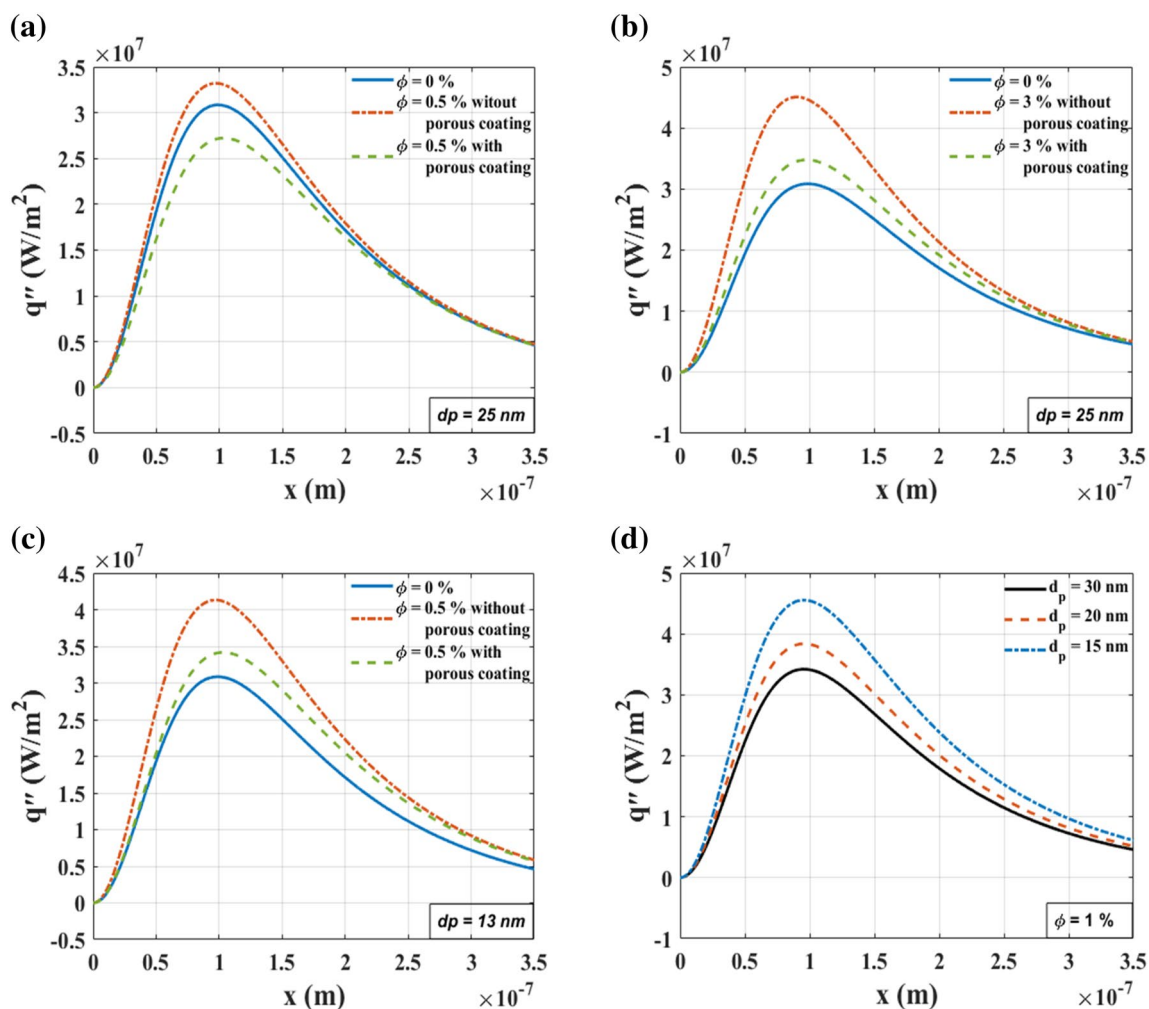
**Fig. 9** **a–c** Effect of porous coating layer including the enhanced thermophysical properties on heat flux with different volumetric fractions ($\phi$) and different average diameter of nanoparticles ($d_p$), **d** effect of average size of nanoparticles ($d_p$) on heat flux at a given volumetric fraction ($\phi$)
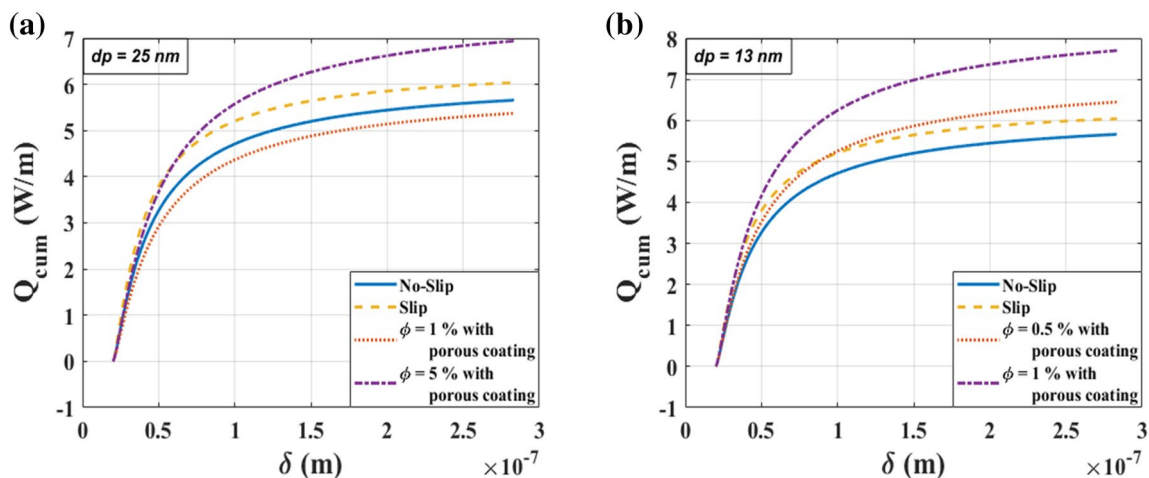


**Fig. 10** Cumulative heat transfer considering the effect of wall slip ($\beta = 5$ nm) and nanofluid incorporation with porous coating layer with different volumetric fractions ($\phi$) and different average diameter of nanoparticles ($d_p$)

can acquire the increment in the heat transfer only if higher $\phi$ is used (Fig. 10a).

The increment in the cumulative heat transfer with respect to the water, with slip, is about 15% only for $\phi = 5\%$. However, an adequate increment in the total heat transfer can also be obtained for the lower volumetric concentration when smaller size of the nanoparticles ($d_p = 13$ nm) is used (Fig. 10b). It is observed that about 27% of increment in the cumulative heat transfer can be obtained using (water + Al$_2$O$_3$) nanofluid with volumetric fraction of just 1% when compared with the base liquid water with slip condition. It can also be inferred from Fig. 10 that with the consideration of wall slip effect ($\beta = 5$ nm), and volumetric fraction of 1%, a decrement in the cumulative heat transfer is observed for larger size nanoparticles ($d_p = 25$ nm), while for the smaller size nanoparticles ($d_p = 13$ nm), a significant increase of 27% in the heat transfer can be noticed. It can also be inferred that for $d_p = 13$ nm, even smaller concentration of nanoparticles ($\phi = 0.5\%$) can increase the heat transfer, which is not true for $d_p = 25$ nm. In addition, Fig. 10 emphasizes the fact that for $d_p = 25$ nm with $\phi$ as high as 5%, shows an increment of cumulative heat transfer by 15%, which is even lesser as compared to the nanofluids with $d_p = 13$ nm and $\phi = 1\%$. Hence, it can be summarized with the aforementioned results that inclusion of nanofluid may have a dual effect on the evaporating meniscus as porous coating layer of nanoparticle may reduce the heat transfer even with the increased thermophysical properties. In addition, for the worthwhile results, smaller sized nanoparticles with higher volume fraction are best suited.

## 4 Conclusions

The combined effects of enhanced thermophysical properties and a porous coating layer of nanoparticles along with the consequences of the slip effect at the wall on the thin-film evaporating dynamics are delineated. To achieve this, an improved mathematical model is used to predict the essential insight of thin-film evaporation with nanofluid incorporation (water–Al$_2$O$_3$), and the comparisons have been made with the base liquid water with and without the effect of wall slip. The following are the findings through the numerical investigation:

- Effective wall slip can reduce the thin-film thickness and enhance the spreading of the working liquid in the evaporating region which in turn, increases the cumulative heat transfer. Consequently, it must be included while explicating the physics of a thin-film evaporating meniscus in a microfluidic channel.
- Nanofluid in comparison with base fluid has shown a tendency to increase the heat transfer from an evaporating thin-film region even though the increase in thickness increases the thermal resistance, because the percentage increment in the thermal conductivity surpasses the percentage increase in the thickness of the thin film.
- The enhanced thermophysical property due to nanofluid, particularly thermal conductivity is a crucial parameter that enhances the heat transfer remarkably without making a significant change in the shape of the evaporating meniscus.
- Nanofluid incorporation exaggerates the increase in heat flux, when enhanced thermophysical properties are considered with no porous coating layer of nanoparticles. The coated layer of nanoparticles can even reduce the heat transfer phenomenon due to the increased layer thickness which directly increases the thermal resistance through it.
- For a given combination of nanoparticle diameter and volume fraction, increase in the thermal resistance may reach up to an extent that even increased thermal conductivity cannot counteract it and hence, the heat transfer obtained using nanofluid can be worse than the heat transfer obtained using the base liquid water alone.
- Selection of the size of the nanoparticle and the volume concentration should be made with careful deliberation to avoid the adverse consequences. Moreover, it is necessary to consider the effect of the porous coating layer with enhanced thermophysical properties of nanofluid to acquire the actual and optimal results.

## References

Biswal L, Som SK, Chakraborty S (2011) Thin film evaporation in microchannels with interfacial slip. Microfluid Nanofluid 10:155–163

Chakraborty S, Som SK (2005) Heat Transfer in an evaporating thin liquid film moving slowly along the walls of an inclined microchannel. Int J Heat Mass Transf 48:2801–2805

Chen G (1996) Nonlocal and non-equilibrium heat conduction in the vicinity of nanoparticles. J Heat Transf 118:539–545

Choi SUS, Eastman JA (1995) Enhancing thermal conductivity of fluids with nanoparticles. In: Singer DA, Wang HP (eds) Development and applications of non-newtonian flows, FED-vol. 231/MD-vol. 66, ASME, New York, pp 99–106

Chon CH, Paik S, Tipton JB, Kihm KD (2007) Effect of nanoparticle sizes and number densities on the evaporation and dryout characteristics for strongly pinned nanofluid droplets. Langmuir 23(6):2953–2960

Das SK, Putra N, Thiesen P, Roetzel W (2003) Temperature dependence of thermal conductivity enhancement for nanofluids. J Heat Transfer 125:567–574

DasGupta S, Schonberg JA, Wayner PC Jr (1993) Investigation of an evaporating extended meniscus based on the augmented young-laplace equation. J Heat Transf 115:201–208

Do KH, Jang SP (2010) Effect of nanofluids on the thermal performance of a flat micro heat pipe with a rectangular grooved wick. Int J Heat Mass Transf 53:2183–2192

Du SY, Zhao YH (2011) New boundary conditions for the evaporating thin-film model in a rectangular micro channel. Int J Heat Mass Transf 54(15–16):3694–3701

Dwivedi R, Singh PK (2018) Decisive influence of nanofluid on thin evaporating meniscus. AIP Conf Proc 1988:020043

Dwivedi R, Singh PK (2019) Numerical analysis of an evaporating thin film region: enticing influence of nanofluid. Numer Heat Transf Part A 75:56–70

Fan J, Wang L (2011) Review of heat conduction in nanofluids. J Heat Transf 133:040801–040814

Fu B, Zhao N, Tian B, Corey W, Ma H (2018) Evaporation heat transfer in thin-film region with bulk vapor flow effect. J Heat Transf 140:011502

Gad-el-Hak M (2001) Flow physics in MEMS. Mécanique Ind 2:313–341

Gatapova EY, Kabov OA (2007) Slip effect on shear-driven evaporating liquid film in microchannel. Micrograv Sci Tech 19:132–134

Hanchak MS, Vangsness MD, Byrd LW, Ervin JS (2014) Thin film evaporation of n-octane on silicon: experiments and theory. Int J Heat Mass Transf 75:196–206

Hanchak MS, Vangsness MD, Ervin JS, Byrd LW (2016a) Model and experiments of the transient evolution of a thin, evaporating liquid film. Int J Heat Mass Transf 92:757–765

Hanchak MS, Vangsness MD, Ervin JS, Byrd LW (2016b) Transient measurement of thin liquid films using a Shack–Hartmann sensor. Int Commun Heat Mass Transf 77:100–103

Holm FW, Goplen SP (1979) Heat transfer in the meniscus thin-film transition region. J Heat Transf 101:498–503

Hu H, Sun Y (2016) Effect of nanostructures on heat transfer coefficient of an evaporating meniscus. Int J Heat Mass Transf 101:878–885

Hwang KS, Jang SP, Choi SUS (2009) Flow and convective heat transfer characteristics of water-based Al$_2$O$_3$ nanofluids in fully developed laminar flow regime. Int J Heat Mass Transf 52:193–199

Jang SP, Choi SUS (2004) Role of Brownian motion in the enhanced thermal conductivity of nanofluids. Appl Phys Lett 84:4316–4318

Jiao AJ, Riegler R, Ma HB, Peterson GP (2005) Thin film evaporation effect on heat transport capability in a grooved heat pipe. Microfluid Nanofluid 1:227–233

Kou ZH, Bai ML (2011) Effects of wall slip and temperature jump on heat and mass transfer characteristics of an evaporating thin film. Int Commun Heat Mass Transf 38:874–878

Kou ZH, Lv HT, Zeng W, Bai ML, Lv JZ (2015) Comparison of different analytical models for heat and mass transfer characteristics of an evaporating meniscus in a micro-channel. Int Commun Heat Mass Transf 63:49–53

Kundu PK, Chakraborty S, DasGupta S (2011) Experimental investigation of enhanced spreading and cooling from a microgrooved surface. Microfluid Nanofluid 11:489–499

Lee S, Choi SUS, Li S, Eastman JA (1999) Measuring thermal conductivity of fluids containing oxide nanoparticles. J Heat Transf 121:280–289

Lim E, Hung YM (2015) Thermophysical phenomena of working fluids of thermocapillary convection in evaporating thin liquid films. Int Commun Heat Mass Transf 60:203–211

Liu ZH, Yang XF, Guo GL (2007a) Effect of nanoparticles in nanofluid on thermal performance in a miniature thermosyphon. J Appl Phy 102(1):013526

Liu ZH, Xiong JG, Bao R (2007b) Boiling heat transfer characteristics of nanofluids in a flat heat pipe evaporator with micro-grooved heating surface. Int J Multiphase Flow 33(12):1284–1295

Ma HB, Cheng P, Borgmeyer B, Wang YX (2008) Fluid flow and heat transfer in the evaporating thin film region. Microfluid Nanofluid 4:237–243

Mandel R, Shooshtari A, Ohadi M (2017) Thin-film evaporation on microgrooved heatsinks. Numer Heat Transf Part A 71:111–127

Moosman S, Homsy GM (1980) Evaporating menisci of wetting fluids. J Colloid Int Sci 73(1):212–223

Narayanan S, Fedorov AG, Joshi YK (2009) Gas-assisted thin-film evaporation from confined spaces for dissipation of high heat fluxes. Nanoscale Microscale Thermophys Eng 13:30–53

Nikolov A, Kondiparty K, Wasan D (2010) Nanoparticle self-structuring in a nanofluid film spreading on a solid surface. Langmuir Lett 26:7665–7670

Ozerinc S, Kakac S, Yazicioglu AG (2010) Enhanced thermal conductivity of nanofluids: a state-of-the-art review. Microfluid Nanofluid 8:145–170

Panchamgam SS, Chatterjee A, Plawsky JL, Wayner PC Jr (2008) Comprehensive experimental and theoretical study of fluid flow and heat transfer in a microscopic evaporating meniscus in a miniature heat exchanger. Int J Heat Mass Transf 51:5368–5379

Park K, Noh KJ, Lee KS (2003) Transport phenomena in the thin-film region of a micro-channel. Int J Heat Mass Transf 46:2381–2388

Pati S, Som SK, Chakraborty S (2013) Combined influences of electrostatic component of disjoining pressure and interfacial slip on thin film evaporation in nanopores. Int J Heat Mass Transf 64:304–312

Poplaski LM, Benn SP, Faghri A (2017) Thermal performance of heat pipes using nanofluids. Int J Heat Mass Transf 107:358–371

Potash M, Wayner PC (1972) Evaporation from a two-dimensional extended meniscus. Int J Heat Mass Transf 15:1851–1863

Ranjan R, Murthy JY, Garimella SV (2011) A microscale model for thin-film evaporation in capillary wick structures. Int J Heat Mass Transf 54(1–3):169–179

Sait HH, Ma HB (2009) An experimental investigation of thin-film evaporation. Nanoscale Microscale Thermophys Eng 13:218–227

Schonberg JA, Wayner PC Jr (1992) Analytical solution for the integral contact line evaporative heat sink. J Thermophys Heat Transf 6:128–134

Schonberg JA, DasGupta S, Wayner PC Jr (1995) An augmented young-laplace model of an evaporating meniscus in a microchannel with high heat flux. Exp Therm Fluid Sci 10:163–170

Schrage RW (1953) A theoretical study of interphase mass transfer. Columbia University Press, New York

Shima PD, Philip J, Raj B (2009) Role of microconvection induced by Brownian motion of nanoparticles in the enhanced thermal conductivity of stable nanofluids. Appl Phys Lett 94:223101

Shkarah AJ, Bin Sulaiman MY, Bin HJ, Ayob M (2015) Analytical solutions of heat transfer and film thickness with slip condition effect in thin-film evaporation for two-phase flow in microchannel. Math Probl Eng 1:2015

Singh PK, Anoop KB, Sundararajan T, Das SK (2010) Entropy generation due to flow and heat transfer in nanofluids. Int J Heat Mass Transf 53:4757–4767

Suman B (2008) Effects of a surface-tension gradient on the performance of a micro-grooved heat pipe: an analytical study. Microfluid Nanofluid 5:655–667

Tesfai W, Singh PK, Masharqa SJS, Souier T, Chiesa M, Shatilla Y (2012) Investigating the effect of suspensions nanostructure on the thermophysical properties of nanofluids. J Appl Phys 112:114315

Tiwary B, Kumar R, Lee PS, Singh PK (2019) Numerical investigation of thermal and hydraulic performance in novel oblique geometry using nanofluid. Numer Heat Transf Part A 76:533–551

Tretheway DC, Meinhart CD (2002) Apparent fluid slip at hydrophobic microchannel walls. Phys Fluids 14:L9–L12

Truong JG, Wayner PC (1987) Effects of capillary and van der waals dispersion forces on the equilibrium profile of a wetting liquid: theory and experiment. J Chem Phys 87:4180–4188

Wang H, Garimella SV, Murthy JY (2007) Characteristics of an evaporating thin film in a microchannel. Int J Heat Mass Transf 50:3933–3942

Wayner PC Jr (1973) Fluid flow in the interline region of an evaporating non-zero contact angle meniscus. Int J Heat Mass Transf 16:1777–1783

Wayner PC Jr, Kao YK, LaCroix LV (1976) The interline heat transfer coefficient of an evaporating wetting film. Int J Heat Mass Transf 19:48–492

Wee SK, Kihm KD, Hallinan KP (2005) Effects of the liquid polarity and the wall slip on the heat and mass transport characteristics of the micro-scale evaporating transition film. Int J Heat Mass Transf 48:265–278

Xuan Y, Li Q (2000) Heat transfer enhancement of nanofluids. Int J Heat Mass Transf 21:58–64

Yan C, Ma HB (2013) Analytical solutions of heat transfer and film thickness in thin-film evaporation. J Heat Transf 135:031501

Yu W, Choi SUS (2003) The role of interfacial layers in the enhanced thermal conductivity of nanofluids: a renovated Maxwell model. J Nanopart Res 5:167–171

Zhao JJ, Duan YY, Wang XD, Wang BX (2011) Effect of nanofluids on thin film evaporation in microchannels. J Nanopart Res 13:5033–5047